Coupling molecular spin centers to microwave planar resonators: towards integration of molecular qubits in quantum circuits†

C. Bonizzoni,*[a,b] A. Ghirri,[b] K. Bader,[c] J. van Slageren,[c] M. Perfetti,[d] L. Sorace,[d] Y. Lan,[e] O. Fuhr,[e] M. Ruben[e,f] and M. Affronte[a,b]

We present spectroscopic measurements looking for the coherent coupling between molecular magnetic centers and microwave photons. The aim is to find the optimal conditions and the best molecular features to achieve the quantum strong coupling regime, for which coherent dynamics of hybrid photon-spin states take place. To this end, we used a high critical temperature YBCO superconducting planar resonator working at 7.7 GHz and at low temperatures to investigate three molecular mononuclear coordination compounds, namely $(PPh_4)_2[Cu(mnt)_2]$ (where mnt^{2-} = maleonitriledithiolate), $[ErPc_2]^-TBA^+$ (where pc^{2-} is the phtalocyaninato and TBA^+ is the tetra-*n*-butylammonium cation) and Dy(trensal) (where H_3trensal = 2,2′,2″-tris(salicylideneimino)triethylamine). Although the strong coupling regime was not achieved in these preliminary experiments, the results provided several hints on how to design molecular magnetic centers to be integrated into hybrid quantum circuits.

Introduction

In the last few years we have been exploring the possibility to coherently manipulate molecular magnetic moments (hereafter also referred to as "molecular spins" for simplicity). The challenge we wish to take up is to move a step ahead with respect to the control of the static magnetic characteristics of molecules and to exploit their genuine quantum features, such as the superposition of molecular states or their quantum correlation (also referred to as "entanglement").[1] However, coherent superposition of states of the systems is fragile since the environment induces decoherence.[2] In this field, key experiments are usually performed with the use of pulsed Electron Paramagnetic Resonance (EPR), which allows the characterization of both spin-lattice relaxation and spin dephasing. The observation of spin echoes is used to test the coherent dynamics of the molecular spin system and to measure the decoherence rates.

We have recently adapted a superconducting planar resonator, which is normally used for circuit-Quantum Electro Dynamics experiments,[3] to manipulate molecular spins with microwave photons.[4] The use of superconductors allows the fabrication of resonators with high quality factor (Q) and typical resonant frequency ($\nu_0 = \omega_0/2\pi$) in the 2–10 GHz range. Such sharp resonances (whose bandwidth is on the order of few hundreds kHz or less) give the possibility to perform EPR spectroscopy with high sensitivity over a wide temperature range.[5,6] By using a photon number which is significantly lower than the number of spins in the sample, it is possible to achieve a different working regime. This is the case in which the collective system is described by the Tavis–Cummings Hamiltonian in terms of hybridized spin-photon states.[7,8] Such coherent dynamics, however, is achieved only when the coupling strength (Ω) between photons and spins exceeds the damping rates of both the resonant cavity ($\kappa_0 = \nu_0/Q$) and spin system (γ). This is generally expressed by the so-called strong coupling condition, $\Omega \gg \kappa_0, \gamma$. While large Ω are relatively easy to achieve with electric dipoles, the coupling to magnetic centers is, in general, much weaker and decoherence mechanisms are still hard to control.[1,3] Some recent experiments have demonstrated that the strong coupling regime can be obtained at very low temperatures ($\ll$1 K). This is the case of electronic spin ensembles provided by Nitrogen Vacancy (NV) centers in diamond[9] or other substitutional spin impurities in

[a]*Dipartimento FIM, Università di Modena e Reggio Emilia, via Campi 213/a, 411125 Modena, Italy. E-mail: claudio.bonizzoni@unimore.it*

[b]*Istituto Nanoscienze - CNR, via Campi 213/a, 411125 Modena, Italy*

[c]*Institut für Physikalische Chemie, Universität Stuttgart, Pfaffenwaldring 55, 70569 Stuttgart, Germany*

[d]*Dipartimento di Chimica "U. Schiff" and UdR INSTM, Università di Firenze, Via della Lastruccia 3-13, 50019 Sesto Fiorentino(FI), Italy*

[e]*Institute of Nanotechnology, Karlsruhe Institute of Technology (KIT),*

D-76344 Eggenstein-Leopoldshafen, Germany

[f]*Institut de Physique et Chimie des Matériaux de Strasbourg, UMR 7504 UdS-CNRS, 67034 Strasbourg Cedex 2, France*

crystals.[10] In particular, Erbium(III) doped crystalline inorganic compound matrices, Er(III):YSi_2O_5 and Er(III):$YAlO_3$, were found to be very interesting for both quantum information and communication.[11] Inspired by these results, we have recently demonstrated that high T_c superconducting resonators can be used to achieve strong coupling with organic radicals[4,12] at finite temperature ($T > 1$ K). The spectroscopic signature for the strong coupling regime is the appearance of two or more distinct branches in the frequency spectrum when the spin system is driven on resonance with the resonator in the low excitation regime.[8,12,13] This is different from ordinary EPR spectroscopy, in which experiments are done in the weak coupling regime and only one single branch is visible.

In the above-mentioned framework, we investigated whether magnetic molecules can be suitable for this type of coherent spin manipulation.[14] A suitable molecular spin system should show: (a) low decoherence, *i.e.* sharp linewidths for the spin transitions, and (b) strong coupling with the magnetic component of the microwave electromagnetic field. With these guidelines in mind, we focused our attention on mononuclear complexes, since molecules with simple structures and nuclear spin free ligands – in principle – suffer less from decoherence, and since sufficiently long coherence times have been recently presented in the literature[15] and are found to be very promising. For instance, mononuclear square planar copper complexes were found to have extraordinary long relaxation times at low-temperatures and quantum coherence even at room temperature.[16] At the same time we wish to enhance the collective coupling. This requires a search for molecules with high transition matrix elements, that is high magnetic coupling to the microwave photons. In this respect, lanthanide-based derivatives look very promising because of their large *g*-factors. Moreover, the possibility to engineer the ligand field through the coordination geometry makes this class of molecules very attractive.

In this work we report a series of preliminary circuit-QED experiments to test the magnetic coupling between selected molecular spin ensembles and a superconducting YBCO coplanar resonator. A mononuclear copper compound, $(PPh_4)_2$-$[Cu(mnt)_2]$ (mnt = maleonitriledithiolate or 1,2-dicyanoethylene-1,2-dithiolate) and two rare-earth-based monometallic SMMs, $[ErPc_2]$ TBA^+ (where pc^{2-} = phtalocyaninato and TBA^+ = tetra-*n*-butylammonium cation, also known as N-nBu_4^+) and Dy(trensal) (H_3trensal = Tris[2-(salicylideneamino)ethyl]amine) with different concentrations and dilutions in diamagnetic analogues are studied. The results are also compared with similar experiments performed with spin impurities in inorganic matrices and organic radicals.

Experimental

Experimental set-up

Transmission spectroscopy experiments were carried out with a high critical temperature YBCO/sapphire coplanar resonator, which was installed into a commercial cryo-magnetic set-up

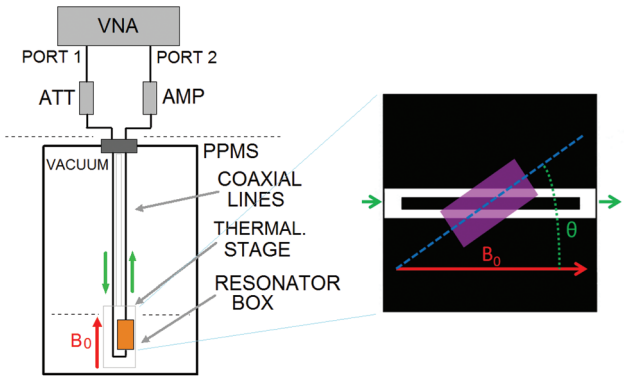

Fig. 1 (Left) Schematic diagram of the experimental set-up. (Right) Top view of the YBCO coplanar resonator (black) with a crystal loaded on top (purple). The red arrow indicates the applied magnetic field, while the green ones indicate the propagation of the TEM microwave signal. θ is the angle between the static magnetic field and the crystal *c*-axis.

(Quantum Design PPMS-7 T) for measurements at varying temperatures and in applied magnetic field (Fig. 1). The transmission scattering parameter (T) was measured as a function of the frequency (ν) by means of a vector network analyzer (Agilent PNA 26 GHz). Measurements at low microwave powers (down to −70 dBm) were carried out with two attenuators and two amplifiers installed at room temperature. The resonator is located in a high-conductivity copper box, where two floating pins inject the microwave field in the coplanar resonator. The extension of the pins can be regulated to adjust the coupling with the external input and output lines. The resonator is located in the centre of the superconducting coil and the magnetic field is applied parallel to the central YBCO strip (Fig. 1). Our resonators are fabricated by optical lithography on YBCO/sapphire films, as reported in ref. 4. The transmission spectrum of the bare resonator shows that $\omega_0/2\pi = 7.764$ GHz and $Q \approx 33\,000$ at 2 K (ESI†). These parameters are remarkably stable in applied magnetic field.[4]

Molecular magnetic complexes

Cu(mnt)$_2$. The coordination compound $(PPh_4)_2[Cu(mnt)_2]$ (where mnt^{2-} = maleonitriledithiolate or 1,2-dicyanoethylene-1,2-dithiolate), hereafter $Cu(mnt)_2$ in short, is shown in Fig. 2. The Cu^{II} ion is coordinated to the sulfur atoms of the two dithiolate ligands, while two PPh_4^+ groups balance the

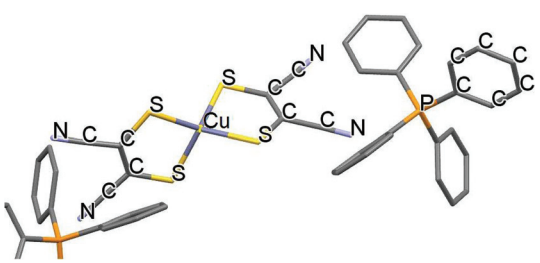

Fig. 2 Crystal structure of the $(PPh_4)_2$**[Cu(mnt)$_2$]** molecule. H atoms are omitted for clarity and the second PPh_4^+ ion is only partially shown.

dinegative charge of the metal complex. $Cu(mnt)_2$ crystallizes in a monoclinic space group with two molecules related by a 2_1 screw axis, leading to two different orientations of the molecules in the unit cell.[17]

The powder EPR spectrum of $Cu(mnt)_2$ [16] shows eight resonance lines resulting from an axial g-tensor and an anisotropic hyperfine interaction between the electron (S = 1/2) and the nuclear spin (I = 3/2) of the two copper isotopes (^{63}Cu, abundance of 69.17%; ^{65}Cu, abundance of 30.83%). The g-factors obtained from the spectral fit are $g_{||}$ = 2.0925 and $g_{\perp}$ = 2.0227.[16]

$[ErPc_2]^-TBA^+$

Single crystals suitable for X-ray diffraction analysis were obtained by slow diffusion of Et_2O into a solution of the $[ErPc_2]$ TBA^+ complex in acetonitrile as fine dark purple needles. This anionic form consists of a trivalent lanthanide ion (Er(III)) coordinated by two Pc ligands, each one bearing a formal charge of −2. The organic core adopts a closed shell π-electronic configuration. The resulting negative charge located on $[ErPc_2]$ is stabilized by a counter cation, such as bulky n-tetrabutylammonium TBA^+. A view of the molecular structure of $[ErPc_2]$ TBA^+ is depicted in Fig. 3(b). The $[ErPc_2]$ TBA^+ complex crystallizes in the orthorhombic space group $Pna2_1$ with four molecules per unit cell which belong to two tilted sub-lattices: a subset of molecules has Pc planes rotated by 10° with respect to the ab plane of the crystal, while the other subset has Pc planes rotated by 160° with respect to the first one (Fig. 3a). This structure was not previously reported in the literature and further details are given in the ESI.†

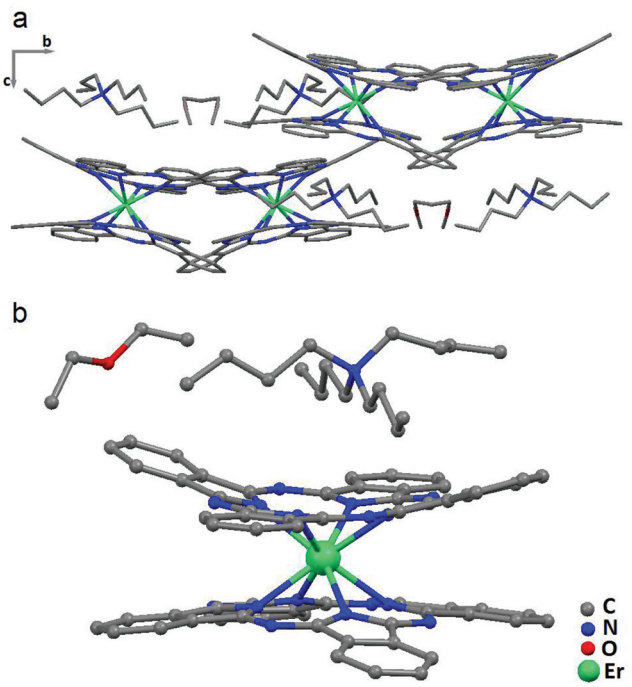

Fig. 3 Molecular structure of $[ErPc_2]^-TBA^+$. Hydrogen atoms are omitted for clarity. (a) Packing diagram of $[ErPc_2]^-TBA^+$, showing the positions of the $[TBA]^+$ cations and diethylether solvent molecules in the unit cell. (b) The molecular structure of $[ErPc_2]^-TBA^+$ showing the Er(III) metal ion (green) coordinated by the isoindole nitrogens (blue).

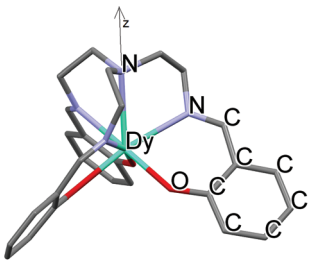

Fig. 4 X-ray structure of the **Dy(trensal)** molecule. Colour scheme: Dy, cyan; O, red; N, violet; C, grey. H atoms are omitted for clarity.

The magnetic properties of the $ErPc_2$ double-decker are characterized by an easy-plane anisotropy, which lifts the degeneracy of the J = 15/2 total angular momentum of the Er^{III} ion. This results in a Kramers M_J = ±1/2 ground doublet, which is well separated from the first excited state (M_J = ±3/2), significantly populated only above 30 K.[18,19] The easy plane anisotropy gives a large effective perpendicular g-factor $g_{\perp}$ = 9.59 in the plane of the phthalocyanines, as reported in ref. 19. Erbium has one isotope with non-zero nuclear spin ^{167}Er (I = 7/2, abundance of 23%) and five isotopes with zero nuclear spin (^{162}Er, ^{164}Er, ^{166}Er, ^{168}Er, ^{170}Er).

Dy(trensal)

Dy(trensal) is a single ion magnet based on Dy(III) bound by the triply deprotonated form of the H_3trensal = 2,2′,2″-tris-(salicylideneimino)triethylamine) ligand (Fig. 4). The system crystallizes in the trigonal $P\bar{3}c1$ space group, in which the Dy(III) and the tertiary aminic nitrogen of the ligand lies on the crystallographic C_3 axis.[20] The molecular symmetry is thus exactly trigonal and the principal anisotropy axis coincides with the crystallographic c axis of the unit cell, as also demonstrated by the low temperature luminescence spectra.[21] Hexagonal, needle-shaped single crystals of Dy(trensal), synthesized as reported for the isostructural Er(III) analogue,[22] typically grow with the crystallographic c axis as the longest dimension of the crystal.[23] The unit cell contains four molecules packed with an enantiomeric displacement and, since the Dy(III) ions lies in a special position, the principal axes of all the molecules are isooriented. The crystal field parameters of Dy(trensal), previously obtained by luminescence spectra[21] and cantilever torque magnetometry[23] revealed the easy plane nature of the magnetic anisotropy of Dy(III) in this molecule. This was further corroborated by the analysis of EPR spectra,[24] providing an anisotropic effective g-tensor with $g_{||}$ = 1.8 along the (hard) z-axis and $g_{\perp}$ = 9.4 in the perpendicular (easy) plane. Dy has 7 stable isotopes (^{156}Dy, ^{158}Dy, ^{160}Dy, ^{161}Dy, ^{162}Dy, ^{163}Dy, ^{164}Dy). Their nuclear spin is I = 0 for the even isotopes, and I = 5/2 for the odd ones.

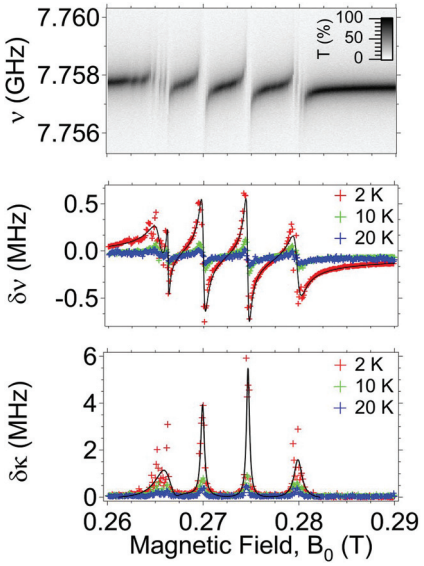

Fig. 5 (Upper panel) Transmission spectral map measured at 2 K for a diluted (2%) and deuterated single crystal of **Cu(mnt)$_2$** (P_{in} = −63 dBm, θ = 0°). (Middle panel) Field dependence of the shift of the resonator frequency and (lower panel) the relative variation of the linewidth. Data taken at 2, 10 and 20 K are shown for comparison. Solid lines display the fitting curve calculated from eqn (1a) and (1b).

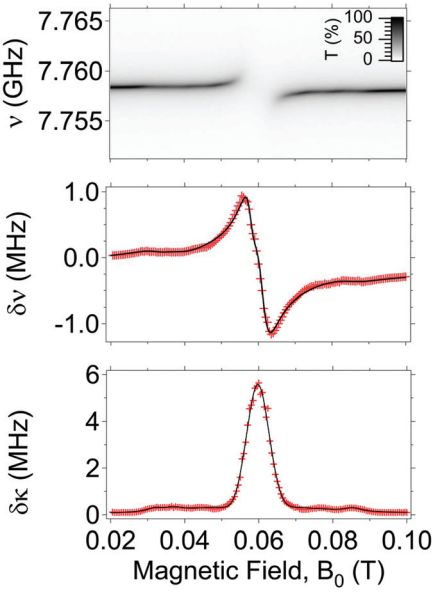

Fig. 6 (Upper panel) Transmission spectral map measured at 2 K for a diluted (10%) **[ErPc$_2$]$^-$TBA$^+$** single crystal (P_{in} = −43 dBm, θ = 90°). (Middle panel) Field dependence of the shift of the resonator frequency and (lower panel) variation of the linewidth. Solid lines display the fitting curve calculated from eqn (1a) and (1b).

Results and discussion

Transmission spectroscopy experiments

For each compound we investigated crystals with different concentrations of magnetic centers and at different orientations with respect to the applied magnetic field. Hereafter we report the main results referring the reader to the ESI† for more complete datasets.

We initially investigated **Cu(mnt)$_2$** single crystals. On a non-diluted Cu(mnt)$_2$ crystal we observed four broad resonances centered at ≈0.27 T which corresponds to a Landé *g*-factor of 2.04 (Fig. S2 of the ESI†). Better resolved structures in the spectrum (Fig. 5) were obtained on a crystal of Cu(mnt)$_2$ doped into the diamagnetic analogue $(PPh_{4\text{-}d20})_2$[Ni(mnt)$_2$] (concentration of *ca.* 2%). The shift of the cavity frequency and the variation of the linewidth are plotted in Fig. 5 as a function of the magnetic field. Lowering the temperature from 20 to 2 K results in a progressive increase of the intensity of the transitions and in their narrowing. The four principal structures can be ascribed to the hyperfine splitting in Cu(mnt)$_2$, which is due to the presence of the nuclear magnetic moment of Cu(II), while the finer structure is due to the fact that two set of molecules with different orientations are present in the crystal. The angular dependence of the measured spectra, reported in Fig. S3 of the ESI,† is consistent with EasySpin simulations carried out with an anisotropic hyperfine Hamiltonian, as discussed in ref. 16.

We investigated single crystals of **[ErPc$_2$]$^-$TBA$^+$** molecules dispersed in the diamagnetic analogue [YPc$_2$] TBA$^+$ with different concentrations. Needle-shaped crystals were aligned with the crystallographic *c*-axis either parallel (θ = 0°) or perpendicular (θ = 90°) to the static magnetic field. Fig. 6 shows the experimental data obtained for a [ErPc$_2$] TBA$^+$ 10% diluted crystal oriented at θ = 90°. For this orientation the two sets of molecules have the same symmetric displacement (10°) of the Pc planes with respect to the external magnetic field. The transmission spectral map shows a resonance at ≈0.061 T (upper panel of Fig. 6), which is accompanied by a shift of the cavity frequency and to an increase of the linewidth (middle and lower panel, respectively). For this resonance, the extracted *g*-factor is ≈9.2, which is consistent with the value reported in ref. 19. The transmission spectra obtained for θ = 0° show the shift of the main resonance toward lower *g*-factors, as it is expected from the easy plane anisotropy of the [ErPc$_2$] TBA$^+$ molecule (Fig. S4 of the ESI†). Other weaker transitions, which are observed in the range between 0.04 and 0.08 T, can be ascribed to the hyperfine components of the magnetic resonance line.

We investigated single-crystals of **Dy(trensal)** dispersed (3%) in isomorphous and diamagnetic Y(trensal). A needle-shaped single crystal was positioned at the centre of the resonator and aligned with the crystallographic *c*-axis perpendicular to the applied magnetic field (θ = 90°). The experimental results are shown in Fig. 7. An intense resonance is measured at ≈0.059 T, which corresponds to $g_\perp \approx 9.4$. Additional weaker resonances, which are located symmetrically with respect to the central one, can be attributed to the hyperfine splitting in $I \neq 0$ Dy isotopes. Measurements taken at θ = 0° show the shift

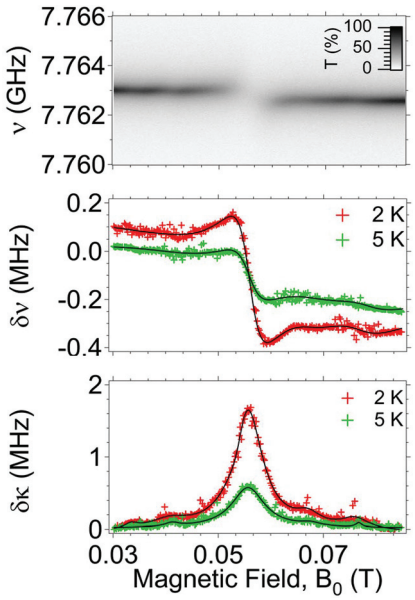

Fig. 7 (Upper panel) Transmission spectral map measured at 2 K for a diluted (3%) single crystal of **Dy(trensal)** (P_{in} = −43 dBm, θ = 90°). (Middle panel) Field dependence of the shift of the resonator frequency and (lower panel) variation of the linewidth. Data taken at 2 and 5 K are shown for comparison. Solid lines display the fitted curve calculated from eqn (1a) and (1b).

of the main resonance to lower *g*-factors, as expected from the easy-plane effective anisotropy of Dy(trensal) (Fig. S6 of the ESI† and ref. 23 and 24).

Discussion

Modelling the magnetic coupling. Within the framework of a lumped elements model, the microwave cavity behaves as a RLC resonator and the coupling with the spin ensemble is introduced through the dynamic susceptibility $\chi = \chi' - i\chi''$, where χ' and χ'' are, respectively, the field-dependent real (dispersion) and imaginary (absorption) parts.[6,25] The susceptibility of the sample affects the inductance as $L'_0 = L_0(1 + \chi'\xi)$ and the resistance as $R'_0 = R_0 + \nu_0 L_0 \xi\chi''$, where L_0 and R_0 are the inductance and the resistance of the bare resonator, respectively. ξ is the filling factor, which takes into account the fraction of the resonator volume filled by the spins. We assume that the bare capacitance (C_0) is unperturbed by χ. The resonant frequency and the quality factor of the resonator become $\nu'_0 = 1/\sqrt{L'_0 C_0} = \nu_0/\sqrt{1+\chi'\xi}$ and $Q'_0 = \nu'_0 R'_0 C_0$, resulting in a linewidth of the resonant peak of $\kappa'_0 = \frac{\nu'_0}{Q'_0}$. Assuming weak coupling ($\chi'\xi \ll 1$) and no saturation, we have:

$$\nu'_0 = \nu_0 + \frac{\Omega^2(\nu_0 - gx)}{(\nu_0 - gx)^2 + \gamma^2} \quad (1a)$$

$$\kappa'_0 = \kappa_0 + \frac{\Omega^2\gamma}{(\nu_0 - gx)^2 + \gamma^2} \quad (1b)$$

Eqn (1) describes the dispersive shift of the resonant peak and its broadening due to the coupling with the spin system respectively. Here, γ is the spin decay rate, g is the Landè *g*-factor (or the effective *g*-factor, g_{eff}, for the lanthanides) and $x = (\mu_B B_0)/h$. The collective coupling strength is:[26]

$$\Omega = g_{eff}\frac{\mu_B}{h}\sqrt{n\int_V \left|\langle G|\vec{b}_{rms}\cdot\vec{S}|E\rangle\right|^2 dV} \quad (2)$$

where $|E\rangle$ and $|G\rangle$ are the excited and ground state coupled by the dipolar magnetic transitions, $\vec{b}_{rms}$ is the vacuum magnetic field of the cavity, n is the (uniform) density of spins and $g_{eff}^2 = g_{(eff,||)}^2\cos^2\theta + g_{(eff,\perp)}^2\sin^2\theta$, where θ is the angle formed by the magnetic anisotropy axis of the molecule with the applied magnetic field. The previous expression can be simplified by introducing the single-spin coupling strength Ω_s, which takes into account the matrix element of the spin transition and the intensity of the magnetic component of the vacuum cavity field.[9–12] In this way, the collective coupling strength simply results to be:

$$\Omega = \Omega_s\sqrt{N_{eff}} \quad (3)$$

where $N_{eff} = nV$ is the number of polarized spins and V is the volume of the sample. The spin density n depends on the temperature according to the Brillouin function, which for spin $\frac{1}{2}$ paramagnets reads[4]

$$n = n_0\tanh\left(\frac{h\nu_0}{2k_BT}\right) \quad (4)$$

where n_0 is the room temperature spin concentration of the crystal. It turns out from eqn (3) and (4) that the effective coupling depends on the concentration of magnetic centers and their polarization at different temperatures.

Data analysis

We now focus our data analysis on the main lines of the respective spectra and we concentrate on the coupling parameters Ω (and Ω_s for a single spin) and on the linewidth γ, which are extracted by fitting curves with eqn (1) and are summarised in Table 1. Notice that the additional hyperfine transitions have, respect to the main resonances, lower intensities and smaller coupling rates, while their linewidths are comparable or even larger. Here we just point out that the decay rate of our resonator is $k_0 \approx 0.3$ MHz [ESI†], which always fulfils the condition $\Omega > k_0$. In addition, the mean cavity photon number spans from $\approx 10^{11}$ (P_{in} = −13 dBm) down to $\approx 10^5$ (P_{in} = −73 dBm) thus the weak excitation limit, $N_{eff} \gg n$, is always satisfied in our experiments.

In comparison with the lanthanide complexes investigated here, the magnetic transitions in a diluted (2%) and deuterated **Cu(mnt)$_2$** single crystal show a sharper linewidth, which is about 6 MHz at 2 K for the main line (Table 1). For this particular resonance, the extracted value of the collective coupling strength is Ω = 2.73 MHz. Taking into account the estimated number of polarized spins, $N_{eff} \approx 7.4 \times 10^{14}$, the single-spin coupling strength results Ω_s = 0.1 Hz. This value is lower than

Table 1 Summary of the parameters extracted by fitting the experimental data with eqn (1a) and (1b). The values reported in the table correspond to the most intense line observed for each molecule. For each compound, the reported line is also the one with the lowest value of linewidth (θ = 0° for $Cu(mnt)_2$ and θ = 90° for the two lanthanide-based complexes)

Sample	*g*-Factor	γ (MHz)	N_{eff} (T = 2 K)	Ω (MHz)	Ω_s (Hz)
$Cu(mnt)_2$ 2%	2.04 ± 0.01	6.2 ± 0.5	7.4×10^{14}	2.7 ± 0.5	0.10 ± 0.05
$[ErPc_2]^-TBA^+$ 10%	9.21 ± 0.01	410 ± 10	6.5×10^{14}	27.1 ± 3.0	1.0 ± 0.2
Dy(trensal) 3%	9.93 ± 0.02	471 ± 38	8×10^{13}	16.2 ± 2.0	1.8 ± 0.3

that obtained for DPPH organic radicals (0.6 Hz) in the same experimental conditions.[4] We attribute this difference to the hyperfine splitting in $Cu(mnt)_2$, which results in the molecules being distributed over four hyperfine levels, thus decreasing the effective number of molecules effectively excited at each resonance.

The comparison between the parameters of $Cu(mnt)_2$ and those of **$[ErPc_2]^-TBA^+$** and **Dy(trensal)** shows larger values of the collective coupling strength for the lanthanides (Table 1). For $[ErPc_2]$ TBA^+ (θ = 90°), we extracted Ω = 27.1 MHz from the fit of the experimental data (Fig. 6). Given the estimated number of polarized spins $N_{eff} = 6.5 \times 10^{14}$, from eqn (3) we obtain Ω_s = 1 Hz. A similar result is obtained for Dy(trensal) (θ = 90°), for which the fit of the experimental curves in Fig. 7 yields $\Omega \approx$ 16.2 MHz, which leads to Ω_s = 1.8 Hz assuming $N_{eff} = 8 \times 10^{13}$ in eqn (3). On the other hand, the fitted linewidths provide 410 MHz and 471 MHz for $[ErPc_2]$ TBA^+ and Dy(trensal), respectively. These values are far larger than those obtained for $Cu(mnt)_2$ and, consequently, the ratio Ω/γ results smaller for the lanthanide molecules. Experiments with less concentrated $[ErPc_2]$ TBA^+ and Dy(trensal) crystals did not show a significant reduction of the measured linewidths. This suggests that the main limitation in our experiments is probably related to the inhomogeneous broadening (see Fig. 7 of the ESI†).

We can conclude that for the 2% diluted and deuterated **$Cu(mnt)_2$** crystal the estimated value of the collective coupling strength results approximately 2.3 times smaller than the linewidth, thus below the strong coupling regime although not very far from it. The **$[ErPc_2]^-TBA^+$** and **Dy(trensal)** samples used in our experiments are still further away from the strong coupling regime with our YBCO resonator, in spite of the their enhanced single-spin coupling strength. Notice that the transitions reported in Table 1 for the lanthanide single-ion molecules are obtained by applying the magnetic field about the easy plane of magnetization, as indicated by the large *g*-factor. The magnetic component of the microwave field, which oscillates perpendicular to the YBCO central strip, is thus applied along the hard direction. According to ref. 11 and eqn (2), higher coupling strengths should be obtained in the orthogonal direction (external magnetic field in the hard direction and microwave field in the easy plane). However, our results reported in Fig. S4, S6 and Tables S1, S2 of the ESI† show weaker intensities and broader lines for these transitions.

Fig. 8 summarizes the main results obtained in our experiments in terms of the coupling rate Ω and the spin linewidth γ. The $\Omega = \gamma$ dashed line is depicted to show the threshold between the weak and strong coupling regimes. Since $\gamma, \Omega > \kappa_0$, these can be simply visualized below and above the $\Omega = \gamma$ dashed line, respectively. For the sake of comparison we add in Fig. 8 the results obtained with DPPH (ref. 4) and PyBTM (ref. 12) organic radicals in similar experimental conditions. Further results reported in the literature for nitrogen vacancy centers in diamond,[9] phosphorus donors in silicon[10] and Er ions in Y_2SiO_5 and in $YAlO_3$[6,11] are also shown for comparison.

The effect of lowering concentration certainly helps in getting sharper lines, but the collective coupling strength is also scaled down with the number of spin centers (eqn (3)) and the total benefit seems to be washed out for certain values of dilution. As an example, for the 2% **$Cu(mnt)_2$** (which has the advantages given by deuteration[16]), concentration values of $\approx 10^{15}$–10^{16} spin per cm^3 are needed to obtain γ below 10 MHz. However, such low concentrations make the collective coupling and the signal too low in our experiments. Rare earth-based compounds have higher spin densities, on the order of $\approx 10^{17}$–10^{19} spin per cm^3 for concentrations from 0.6% to 3%. This

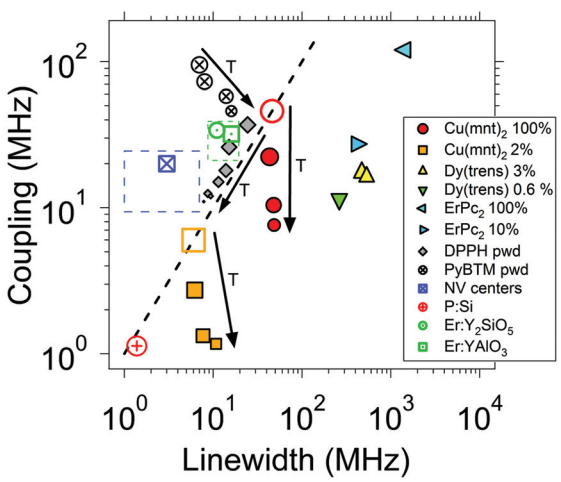

Fig. 8 Plot of coupling rate and spin linewidth parameters obtained by fitting the experimental data with eqn (1) (filled symbols). Data taken at different temperatures are indicated by the black arrows and by symbols of different sizes that range from 2 K (larger symbols) to 50 K (smaller symbols). Empty symbols display the parameters extrapolated to 0.3 K by means of eqn (4). The dashed line indicates $\Omega = \gamma$. The parameters of DPPH and PyBTM organic radicals are taken from ref. 4 and 12 respectively. Additional points from ref. 9–11 are shown for comparison. Dashed rectangles show the typical working ranges obtained for NV centers (blue) and Er ions in inorganic crystals (green) coupled to superconducting Niobium planar resonators at temperatures between 10 and 50 mK.

gives both higher number of spins and higher coupling rates with respect to $Cu(mnt)_2$ but, at the same time, higher dipolar interactions and heavier broadening effects. On the contrary, NV centers have typical spin densities of $\approx 10^{17}$–10^{18} spin per cm^3 but with doping percentages (*i.e.* concentration of spin impurities) from 0.006% to 0.01%.[9] Similar spin density values hold also for Er-doped crystals, whose typical concentrations span from 0.005% to 0.02%.[11] It's clear that magnetic impurities in crystals can reach higher dilutions with respect to molecular spins while maintaining a comparable or higher spin density. This helps both in the reduction of line broadening effects and in reaching high coupling rates. Despite this intrinsic limit, **$Cu(mnt)_2$** samples at 2 K show comparable linewidths with respect to the ones of NV centers and Er ions but at 10–50 mK. This is very interesting, especially after thinking that the temperature is about 100 times higher and the fact that molecular spins have more complex molecular structures with respect to solid-state electronic spins. In addition, the linewidths of $Cu(mnt)_2$ samples are comparable or even lower with respect to the ones of organic radicals, in which exchange narrowing[4,12] contributes to the reduction of the spin linewidth.

Furthermore, we consider the effect of the temperature. For this, we plot in Fig. 8 the fitted Ω and γ of our samples at different temperatures between 2 and 70 K, at which experiments were systematically repeated. As expected, lowering the temperature increases the collective coupling Ω, since the number of polarized spin increases (eqn (4)) and, at the same time, the linewidths get slightly sharper. Both effects may eventually lead to the strong coupling regimes. By simply extrapolating the curves in Fig. 8 we can estimate that working at 0.3 K could allow one to achieve strong coupling with the $Cu(mnt)_2$ samples. Notice that this temperature is about 10 times higher with respect to the typical temperatures used for NV-centers and Er ions thus showing that molecular spin centers can actually be competitive with respect to spin defects in inorganic solids.

Conclusions

In conclusion we investigated different molecular magnetic centers at low temperatures by means of superconducting YBCO resonators looking for the strong coupling regime. The collective coupling Ω and the spin linewidth γ were systematically investigated for different dilutions and orientations of the magnetic centers. Lanthanide-based molecules were found to have not only high coupling strengths but also the broadest spin linewidths. Mononuclear molecular $Cu(mnt)_2$ compounds can have comparable linewidths with respect to the typical values reported for NV centers and Er ions in crystals. In particular, the 2% deuterated $Cu(mnt)_2$ was found to have the minimum linewidth of 6 MHz. Despite this, the coupling strength at 2 K is not sufficient to achieve the strong coupling regime, although not very far from it.

The origin of the main limitation in reducing the essential parameter γ of our experiments still needs to be clarified: on one hand, single molecule relaxation and coherence times T_1 and T_2 both contribute to the collective linewidth γ. On the other hand inhomogeneous broadening also plays a role in the final results. In the case of $[ErPc_2]$ TBA^+ part of the line broadening comes from the convolutions of two resonances related to the two orientations of molecules in the crystalline structure. Furthermore, isotopic enrichment performed on the even rare earth isotopes ($I = 0$) could help in the reduction of hyperfine contributions to the main lines. These issues need to be controlled in a better way in order to design new molecular crystals suitable for circuit-QED experiments.

Acknowledgements

We wish to thank S. Carretta (University of Parma) and D. Gerace (University of Pavia) for useful discussion, and S. Klyatskaya (Karlsruhe Institute of Technology) for additional $[ErPc_2]$ TBA^+ sample preparation and characterization and acknowledge the KNMF facility (KIT, Germany) for the allocation of technical equipment. This work was partially funded by the Italian Ministry of Education and Research (MIUR) through the "Fondo Investimenti per la Ricerca di Base" (FIRB) Project RBFR12RPD1, by the U.S. AFOSR/AOARD program, contract no. FA2386-13-1-4029 and by the European FP7 FET project MoQuaS contract N. 610449.

References

1 A. Ghirri, F. Troiani and M. Affronte, in *Molecular Nanomagnets and Related Phenomena - Structure and Bonding*, ed. S. Gao, Springer, Berlin, 2015.

2 P. C. E. Stamp and A. Gaita-Ariño, *J. Mater. Chem.*, 2009, **19**, 1718–1730.

3 Z.-L. Xiang, S. Ashhab, J. Q. You and F. Nori, *Rev. Mod. Phys.*, 2013, **85**, 623.

4 A. Ghirri, C. Bonizzoni, D. Gerace, S. Sanna, A. Cassinese and M. Affronte, *Appl. Phys. Lett.*, 2015, **106**, 184101.

5 A. Bienfait, J. J. Pla, Y. Kubo, M. Stern, X. Zhou, C. C. Lo, C. D. Weis, T. Schenkel, M. L. W. Thewalt, D. Vion, D. Esteve, B. Julsgaard, K. Mølmer, J. J. L. Morton and P. Bertet, *Nat. Nanotechnol.*, 2016, **11**, 253; G. Boero, G. Gualco, R. Lisowski, J. Anders, D. Suter and J. Brugger, *J. Magn. Reson.*, 2013, **231**, 133–140; G. Gualco, J. Anders, A. Sienkiewicz, S. Alberti, L. ForrÓ and G. Boero, *J. Magn. Reson.*, 2014, **247**, 96–103; H. Malissa, D. I. Schuster, A. M. Tyryshkin, A. A. Houck and S. A. Lyon, *Rev. Sci. Instrum.*, 2013, **84**, 025116; O. Benningshof, H. Mohebbi, I. Taminiau, G. Miao and D. Cory, *J. Magn. Reson.*, 2013, **230**, 84–87.

6 P. Bushev, A. K. Feofanov, H. Rotzinger, I. Protopopov, J. H. Cole, C. M. Wilson, G. Fischer, A. Lukashenko and A. V. Ustinov, *Phys. Rev. B: Condens. Matter*, 2011, **84**, 060501(R).

7 Z. Kurucz, J. H. Wesenberg and K. Molmer, *Phys. Rev. A*, 2011, **83**, 053852; I. Diniz, S. Portolan, R. Ferreira, J. M. Gerard, P. Bertet and A. Auffeves, *Phys. Rev. A*, 2011, **84**, 063810.

8 I. Chiorescu, N. Groll, S. Bertaina, T. Mori and S. Myiashita, *Phys. Rev. B: Condens. Matter*, 2010, **82**, 024413.

9 Y. Kubo, F. R. Ong, P. Bertet, D. Vion, V. Jacques, D. Zheng, A. Dreau, J. F. Roch, A. Auffeves, F. Jelezko, J. Wrachtrup, M. F. Barthe, P. Bergonzo and D. Esteve, *Phys. Rev. Lett.*, 2010, **105**, 140502; D. I. Schuster, A. P. Sears, E. Ginossar, L. DiCarlo, L. Frunzio, J. J. L. Morton, H. Wu, G. A. D. Briggs, B. B. Buckley, D. D. Awschalom and R. J. Schoelkopf, *Phys. Rev. Lett.*, 2010, **105**, 140501; R. Amsuss, C. Koller, T. Nobauer, S. Putz, S. Rotter, K. Sandner, S. Schneider, M. Schrambock, G. Steinhauser, H. Ritsch, J. Schmiedmayer and J. Majer, *Phys. Rev. Lett.*, 2011, **107**, 060502.

10 J. J. Morton and B. W. Lovett, *Annu. Rev. Condens. Matter Phys.*, 2011, **2**, 189–212; C. W. Zollitsch, K. Mueller, D. P. Franke, S. T. B. Goennenwein, M. S. Brandt, R. Gross and H. Huebl, *Appl. Phys. Lett.*, 2015, **107**, 142105.

11 S. Probst, H. Rotzinger, S. Wunsch, P. Jung, M. Jerger, M. Siegel, A. V. Ustinov and P. A. Bushev, *Phys. Rev. Lett.*, 2013, **110**, 157001; A. Tkalčec, S. Probst, D. Rieger, H. Rotzinger, S. Wünsch, N. Kukharchyk, A. D. Wieck, M. Siegel, A. V. Ustinov and P. Bushev, *Phys. Rev. B: Condens. Matter*, 2014, **90**, 075112.

12 A. Ghirri, C. Bonizzoni, F. Troiani, N. Buccheri, L. Beverina, A. Cassinese and M. Affronte, *Phys. Rev. A.*, 2016, **93**, 063855.

13 E. Abe, H. Wu, A. Ardavan and J. J. L. Morton, *Appl. Phys. Lett.*, 2011, **98**, 251108.

14 A. W. Eddins, C. C. Beedle, D. N. Hendrickson and J. R. Friedman, *Phys. Rev. Lett.*, 2014, **112**, 120501.

15 M. Warner, S. Din, I. S. Tupitsyn, G. W. Morley, A. M. Stoneham, J. A. Gardener, Z. Wu, A. J. Fisher, S. Heutz, C. W. M. Kay and G. Aeppli, *Nature*, 2013, **503**, 504; J. M. Zadrozny, J. Niklas, O. G. Poluektov and D. E. Freedman, *ACS Cent. Sci.*, 2015, **1**, 488; M. Atzori, L. Tesi, E. Morra, M. Chiesa, L. Sorace and R. Sessoli, *J. Am. Chem. Soc.*, 2016, **138**, 2154; L. Tesi, E. Lucaccini, I. Cimatti, M. Perfetti, M. Mannini, M. Atzori, E. Morra, M. Chiesa, A. Caneschi, L. Sorace and R. Sessoli, *Chem. Sci.*, 2016, **7**, 2074–2083.

16 K. Bader, D. Dengler, S. Lenz, B. Endeward, S.-D. Jiang, P. Neugebauer and J. van Slageren, *Nat. Commun.*, 2014, **5**, 5304.

17 G. R. Lewis and I. Dance, *J. Chem. Soc., Dalton Trans.*, 2000, 3176.

18 N. Ishikawa, M. Sugita, T. Okubo, N. Tanaka, T. Iino and Y. Kaizu, *Inorg. Chem.*, 2003, **42**, 2440.

19 R. Marx, F. Moro, M. Dorfel, L. Ungur, M. Waters, S. D. Jiang, M. Orlita, J. Taylor, W. Frey, L. F. Chibotaru and J. van Slageren, *Chem. Sci.*, 2014, **5**, 3287.

20 M. Kanesato and T. Yokoyama, *Anal. Sci.*, 2000, **16**, 335.

21 B. M. Flanagan, P. V. Bernhardt, E. R. Krausz, S. R. Luthi and M. J. Riley, *Inorg. Chem.*, 2002, **41**, 5024.

22 K. S. Pedersen, L. Ungur, M. Sigrist, A. Sundt, M. Schau-Magnussen, V. Vieru, H. Mutka, S. Rols, H. Weihe, O. Waldmann, L. F. Chibotaru, J. Bendix and J. Dreiser, *Chem. Sci.*, 2014, **5**, 1650.

23 M. Perfetti, E. Lucaccini, L. Sorace, J. P. Costes and R. Sessoli, *Inorg. Chem.*, 2015, **54**, 3090.

24 E. Lucaccini, L. Sorace, M. Perfetti, J.-P. Costes and R. Sessoli, *Chem. Commun.*, 2014, **50**, 1648.

25 A. Abragam and B. Bleaney, *Electron Paramagnetic Resonance of Transition Ions*, Dover, New York, 1986.

26 M. Jenkins, T. Hümmer, M. J. Martínez-Pérez, J. García-Ripoll, D. Zueco and F. Luis, *New J. Phys.*, 2013, 15.